Int. J. Electrochem. Sci., 11 **(2016)** 5364 – 5379, doi: 10.20964/2016.07.76

International Journal of ELECTROCHEMICAL SCIENCE
www.electrochemsci.org

Methanol Electro-Oxidation on Bimetallic PtMo/C Catalysts and Pt/C - Mo/C Mechanical Mixtures

L. C. Ordóñez[1,*], *P. Roquero*[2], *J. Ramírez*[2], *P.J. Sebastian*[3]

[1] Unidad de Energía Renovable-CICY, C. 43 No 130 Col. Chuburná de Hidalgo, Mérida Yucatán, México. CP 97200.
[2] Facultad de Química, Universidad Nacional Autónoma de México, Cd. Universitaria, México D. F. 04510, México.
[3] Instituto de Energías Renovables, Universidad Nacional Autónoma de México, Temixco, Morelos, México. CP 62580.
[*]E-mail: lcol@cicy.mx

Received: 9 July 2015 / *Accepted:* 7 February 2016 / *Published:* 4 June 2016

The role of molybdenum in carbon-supported Pt-Mo electrocatalysts was studied with the aim of obtaining active materials to be used as anodes in the methanol electro-oxidation reaction. The catalysts were synthesized by the thermolysis of Mo and Pt carbonyls. Two series were obtained: bimetallic PtMo/C, and Pt/C plus Mo/C mechanical mixtures. The Mo content was changed, with the atomic ratio ranging from 0.0 to 1.0. XRD and XPS analyses of the fresh materials indicated the presence of Pt^0 and molybdenum oxides (MoO_x). XRD of Mo/C treated electrochemically at constant potential in H_2SO_4 confirmed the formation of molybdenum bronzes with different protonation degrees (H_xMoO_3 $0.3 < x < 2$). Cyclic voltammetry indicated that Mo/C does not present the capacity to oxidize methanol nor the intermediate species, but it did show promoter behavior. In the PtMo/C series, low molybdenum contents present the maximum promoting effect on methanol electro-oxidation, as evidenced by lower onset potentials for the methanol oxidation reaction with respect to the Pt/C catalyst. Similar results were registered by the mechanical mixtures, where the Pt sites are separated from the molybdenum bronzes, suggesting that Pt poisoned sites, caused by methanol electro-adsorption, are cleaned by the interaction with molybdenum bronzes (H_xMoO_3) through a process of surface diffusion of oxygen-containing species.

Keywords: PtMo/C, mechanical mixtures, Pt/C, Mo/C, DMFC, methanol electro-oxidation, electrocatayst.

1. INTRODUCTION

Environmental issues associated with increasing energy demands and extremely high dependence on conventional fossil fuel sources have led to the consideration and research of new energy sources. Direct alcohol fuel cells (DAFC) have attracted attention, since these devices can directly transform the chemical energy of low molecular weight alcohols into electricity through electro-catalytic reactions more efficiently than internal combustion systems. Furthermore, methanol and ethanol possess energy densities similar to that of gasoline (6-9 $kWhkg^{-1}$)[1], can be produced by different methods, and can be stored and transported using the available infrastructure with few modifications.

A direct methanol fuel cell (DMFC) consists of an anode where methanol is electro-oxidized to CO_2 and a cathode at which oxygen, normally from the air, is reduced to form water. The two electrodes, commonly based on platinum, are typically separated by an ion-conducting electrolyte membrane. The complete methanol electro-oxidation reaction (MOR) should yield 6 electrons mol^{-1}, according to:

$$CH_3OH + H_2O \rightarrow CO_2 + 6H^+ + 6e^- \ (E^0 = 0.046 \text{ V vs. NHE})$$

However, this electrochemical reaction exhibits a complex multipathway mechanism where intermediate species such as $(CHO)_{ads}$ or $(COOH)_{ads}$ are formed and eventually become CO [2, 3]. These species strongly adsorb on Pt active sites, poisoning them and causing a decrease in overall fuel cell efficiency.

Significant scientific efforts have focused on the development of electrocatalytic materials with significantly lower affinity for these intermediates, attempting to maintain good activity for the methanol oxidation reaction at the lowest possible potential. Pt has been combined with oxophilic elements, such as Ru, Sn or Mo [4-14], with the intention of producing OH^- surface groups at lower potentials than on Pt alone, which could oxidize the adsorbed species to CO_2.

In the case of Ru, the observed promoting effect has been explained by the combination of both the bifunctional mechanism and the ligand effect [6, 7, 12-15]. In the former, a partially oxidized Ru surface can supply OH^- groups to adjacent Pt sites poisoned with methanol adsorption residues to form CO_2. The ligand effect, or intrinsic electronic mechanism, considers that the presence of Ru or Sn changes the Pt electronic structure, weakening the bonds between intermediate species and Pt active sites [15-18].

Molybdenum is an element with great potential as a promoter for enhancing Pt activity in the MOR. It is inexpensive, widely available and has been tested with good results in this field. Bimetallic PtMo catalysts have been recognized for their excellent catalytic activity in CO, methanol and ethanol electro-oxidation reactions [19-22]. However, there is no definitive explanation of the nature of the Mo promoting effect. Redox couples Mo(VI)/Mo(V)[23] and Mo(VI)/Mo(IV) [24-26] have been related to an improvement in MOR activity. It has also been proposed that molybdenum oxides (MoO_3) or oxyhydroxides [9] capable of adsorbing large quantities of OH^- groups present a bifunctional effect similar to that of Ru. However, contrary to Ru, it has been reported that molybdenum species do not

present affinity towards CO, and Mo surfaces can therefore have a larger number of available sites over a wide potential range to carry out water electro-dissociation, thereby contributing to the generation of OH^- species to oxidize organic intermediates adsorbed at adjacent Pt sites, according to the bifunctional mechanism. It has also been suggested that the presence of Mo could change Pt-Pt atomic distances, thus diminishing the adsorption energy of intermediate species [16]. On the other hand, Pt d-orbital vacancy calculations for PtRu and PtMo indicate that Mo is more easily oxidized than Ru, which is a favorable attribute for the oxidation of CO or other methanol oxidation residues. The improvement in MOR activity has also been attributed to the presence of sub-stoichiometric Mo oxides (MoO_x $2 < x < 3$)[27] that participate in a spillover mechanism, described in heterogeneous catalysis as the movement of the active species adsorbed or formed on one phase to another phase on which they are not adsorbed or generated under the experimental conditions [28, 29]. Species such as H^+, CO or other oxygen-containing species can participate in this surface-diffusion process, by which the global activity of a catalyst can be improved [30, 31]. The proton spillover mechanism has also been suggested to explain the molybdenum promoting effect in the improvement of methanol oxidation at carbon-supported Pt modified with $HxMoO_3$ [32, 33], carbon nanotube-supported Pt modified with H_xMoO_3, Pt decorated with pored-arrayed H_xMoO_3 [34, 35] and Pt-H_xMoO_3-Polyaniline materials [36]. In these studies, it is proposed that H_xMoO_3 with high hydrogen content is easily oxidized to form H_yMoO_3 with lower hydrogen content or even MoO_3, the function of H_yMoO_3 being that of a proton-acceptor to assist the oxidation of methanol or other intermediate species adsorbed on Pt sites, in accordance with:

$$Pt + CH_3OH \rightarrow [CH_zO]_{ads} + (4\text{-}z)\, e^- + (4\text{-}z)\, H^+$$
$$Pt\text{-}[CHzO]_{ads} + Pt\text{-}[H_yMoO_3]_{ads} + H_2O \rightarrow CO_2 + Pt + Pt\text{-}[H_xMoO_3]_{ads}$$
$$Pt\text{-}[H_xMoO_3]_{ads} \rightarrow Pt\text{-}[H_yMoO_3]_{ads} + (x\text{-}y)\, e^- + (x\text{-}y)\, H^+ \quad 0 < y \leq 2$$

Similarly, for the Pt/WO_3 system, Shen P.K. *et al.* [37] proposed that methanol oxidation activity was improved with respect to Pt alone by the formation of a tungsten bronze (H_xWO_3) caused by proton spillover from Pt sites, where methanol is deprotonated, to WO_3 sites, yielding free Pt sites available for methanol adsorption. However, hydrogen adsorption on Pt sites and its surface diffusion is generally a rapid step under normal conditions [10]. On the other hand, oxygen spillover can easily take place on MoO_3 [38]. Thus, an OH^- back-spillover could be favored from $HxMoO_3$ to Pt poisoned sites.

The purpose of this work is to investigate the possible existence of a remote promoting effect of Mo, by comparing the activities of the methanol oxidation reaction at PtMo/C, prepared by simultaneous metal carbonyl thermolysis, with those obtained from mechanical mixtures of the supported monometallic materials: Pt/C and Mo/C.

2. EXPERIMENTAL

2.1 Electrocatalyst synthesis

The synthesis of PtMo/C electrocatalysts was carried out by means of the metal carbonyl thermolysis method, as described in [10, 11, 15, 19-21]. Molybdenum hexacarbonyl ($Mo(CO)_6$) was purchased from Aldrich® and Pt carbonyl complex was synthesized by bubbling CO during 24 h at a volumetric flow rate of 25 $cm^3\ min^{-1}$ through 50 cm^3 of an aqueous chloroplatinic acid solution (10 mg cm^{-3} H_2PtCl_6). The system was subjected to constant stirring until the color changed from orange to cherry red, indicating that the Pt carbonyl had precipitated. This precipitate was filtered and dried under a CO atmosphere. Appropriate quantities of Pt and Mo carbonyl complexes and Vulcan XC72R carbon were placed in a reflux system using o-xylene as solvent. The temperature was increased to the boiling point of o-xylene (140 ºC) and reflux was maintained for 24 h. Once the selected contact time was reached, the solvent was distilled. The catalysts were formulated with 80 wt% carbon and 20 wt% metal content. The active phase composition varied according to the atomic ratio R = Mo/(Mo+Pt) = 0, 0.2, 0.3, 0.5, 0.8 and 1 [19, 21]. Mechanical mixtures of Mo/C plus Pt/C were prepared by introducing the required amounts of both electrocatalysts in a closed flask and applying vigorous mixing for 30 minutes. All prepared materials were subjected to a thermal treatment at 400 °C in N_2 atmosphere for 4 h. Table 1 shows the prepared materials.

Table 1. Prepared materials.

Sample	Atomic ratio R=Mo/(Mo+Pt)	Pt:Mo ratio	Weight %			Catalytic area m^2g^{-1}
			Pt	Mo	Carbon	
PtMo/C series						
Pt/C	0.0	1:0	20	0	80	5.75
Pt9Mo1/C	0.1	9:1	19.0	1.0	80	9.58
Pt4Mo1/C	0.2	4:1	17.8	2.2	80	7.41
Pt7Mo3/C	0.3	7:3	16.5	3.5	80	8.52
Pt1Mo1/C	0.5	1:1	13.4	6.6	80	12.45
Pt1Mo4/C	0.8	1:4	6.7	13.3	80	9.84
Mo/C	1.0	0:1	0	20	80	N.D.
Mechanical mixtures series						
M1	0.2	4:1				3.14
M2	0.3	7:3				6.31
M3	0.5	1:1				2.81
M4	0.8	1:4				4.20

2.2 X-Ray diffraction (XRD)

X-ray diffraction patterns of the fine powder samples packed in a glass holder were recorded at room temperature in a Siemens D-500 diffractometer, using CuK radiation (α = 1.5406 Å) and a speed of 2° min^{-1} [19, 21].

2.3 High-resolution transmission electron microscopy (HRTEM)

The samples were dispersed in n-heptane in an ultrasound bath for 1 h. A few drops of the supernatant liquid were deposited on 200-mesh copper grids covered with a carbon film. Images were obtained with a JEOL 2010 microscope [19, 21]. Z-contrast and elemental analysis of some particles were carried out in order to identify the Pt and Mo distribution on the surface of the support.

2.4 X-Ray photoelectron spectroscopy (XPS)

XPS spectra of the PtMo/C electrocatalysts were recorded in a VG-Scientific Microtech Multilab ESCA2000 ultra-high vacuum spectrometer, equipped with a CLAM4 MCD analyzer and a Mg Kα X-ray source (hν = 1253.6 eV) operated at 15 kV with 20 mA beam intensity. XPS spectra were recorded at 55° with respect to the normal of the sample surface with a constant energy pass mode E0 = 50 eV and 20 eV for survey and high-resolution narrow scan respectively. Samples were compressed into a 10 mm diameter pellet and placed in a vacuum chamber at $5x10^{-8}$ mbar. The pellet surface was etched for 5 minutes with 3 kV Ar^+ at 0.17 μAcm^{-2}. The analysis was performed with the SDPv4.1® software. Binding energies were calibrated with respect to C (1s) at 285 eV with a resolution (FWHM) of 1.0 eV.

2.5 Electrochemical tests

Electrodes were prepared by mixing the appropriate amounts of catalyst powder with i-propanol and a 5 wt% Nafion® solution from Aldrich. This mixture was homogenized in an ultrasonic bath during 15 minutes. 5 μL of this catalytic ink were deposited onto a 5 mm diameter glassy carbon disk electrode. The catalyst loading corresponds to 2.54 mg cm^{-2}, referred to the geometric surface area of the disk [21].

2.6 Electrochemical measurements

The electrochemical experiments were carried out at 25 °C using a Radiometer-50 potentiostat-galvanostat. A typical three-electrode cell was used with a saturated calomel electrode ($Hg/Hg_2Cl_2/KCl_{(sat)}$) as the reference, a graphite bar as the counter electrode and each synthesized material as the working electrode [21]. All electrode potentials throughout this paper are presented with respect to the normal hydrogen electrode scale (NHE). The working solution consisted of 1.0 M methanol and 0.5 M

H_2SO_4 as the supporting electrolyte. Prior to each electrochemical test, the electrode materials were stabilized in a nitrogen-outgassed 0.5 M H_2SO_4 electrolyte by potential cycling from 0.2 to 1.0 V vs. NHE at a scan rate of 50 mVs^{-1} until no changes in electrical current were registered. For the CO-stripping voltammetry experiments, CO was adsorbed on the working electrode surface by fixing the potential at 100 mV for 1 h using a CO-saturated 0.5 M H_2SO_4 working solution. The electrolyte was then replaced by a CO-free, nitrogen-outgassed 0.5 M H_2SO_4 solution and CV tests were carried out in a potential window from 0 to 1.35 V vs. NHE at a scan rate of 10 mVs^{-1} [21, 22]. The system was kept without stirring. All potential sweeps were first carried out towards positive potentials and then reversed towards negative potentials. The catalytic active area was calculated from the electrical charge of the CO oxidation peak, assuming the oxidation of a monolayer of linearly adsorbed CO on Pt sites, which corresponds to a 0.420 $mCcm^{-2}$ charge [21, 22]. Current-sampled voltammetry was carried out in a potential range from 0.0 to 1.2 V vs. NHE. The potential was fixed every 100 mV and current was registered during 30 s. Each stable current value was taken to build I vs. E plots. In order to observe different Mo species formed under different electrochemical conditions, large quantities of Mo/C catalyst were deposited onto a stainless steel mesh electrode, which was used as the working electrode in the three-electrode cell described above using a 0.5 M H_2SO_4 electrolyte solution. After electrochemical treatment at fixed potential for 1 h, the Mo/C sample was separated from the mesh and analyzed by XRD. This procedure was repeated at potentials of -0.158, 0.17, 0.45, 0.7, 1.16 and 2 V vs. NHE.

3. RESULTS AND DISCUSSION

3.1 Physical characterizations

Figure 1 displays the diffraction patterns of fresh and electrochemically treated Mo/C electrocatalyst. Vulcan carbon support exhibits the characteristics of graphite. Fresh Mo/C presents an XDR pattern similar to that of carbon, with a small peak at $2\theta = 26°$ corresponding to the $MoO_{2.88}$ phase (card 09-0195). After the electrochemical treatment, a broad region appears between 15° and 17° 2θ which is related to the formation of $HMo_{5.4}O_{15.8}OH_{1.6}\cdot 17H_2O$ (card 47-0872), $HxMoO_3\cdot H_2O$ (card 37-0519), $MoO_3\cdot H_2O$ (card 28-0666), $MoO_3\cdot 0.34H_2O$ (card 46-1048), $H_{0.93}MoO_3$ (card 33-0605), $H_{0.34}MoO_3$ (card 34-1234) and $H_{1.68}MoO_3$ (card 33-0604). All of these phases are known as molybdenum bronzes and are represented as H_xMoO_3 [39]. They maintain the octahedral crystalline structure of MoO_3 and can be grouped into a series of four simple phases in the range of $0 < x < 2$ [5], named as follows: green monoclinic ($x = 2$), red monoclinic ($1.55 < x < 1.72$), blue monoclinic ($0.85 < x < 1.04$) and blue orthorhombic ($0.23 < x < 0.4$). In phases with high x values, H is present in the form of water ($-OH_2$) or OH^- groups coordinated to Mo atoms located at the end of the lattice [40-43]. The Pt/C electrocatalyst (Figure 2) presents diffraction lines at $2\theta = 39$, 46, 67, 81 and 86°, corresponding respectively to the (1,1,1), (2,0,0), (3,1,1) and (2,2,2) planes of a face-centered cubic crystalline structure (Card 4-0802).

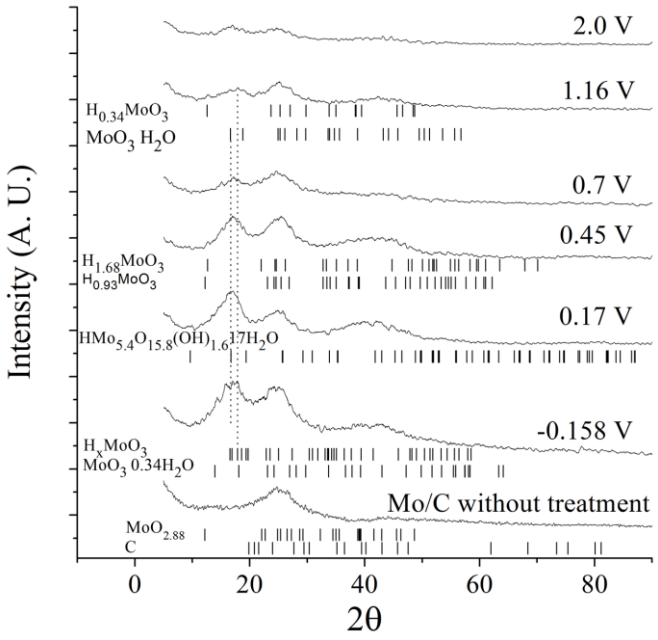

Figure 1. XRD of fresh and electrochemically treated Mo/C. Each treatment was performed for 1 h at fixed potentials of 0.158, 0.17, 0.45, 0.7, 1.16 y 2 V vs NHE using 0.5 M H_2SO_4 supporting electrolyte.

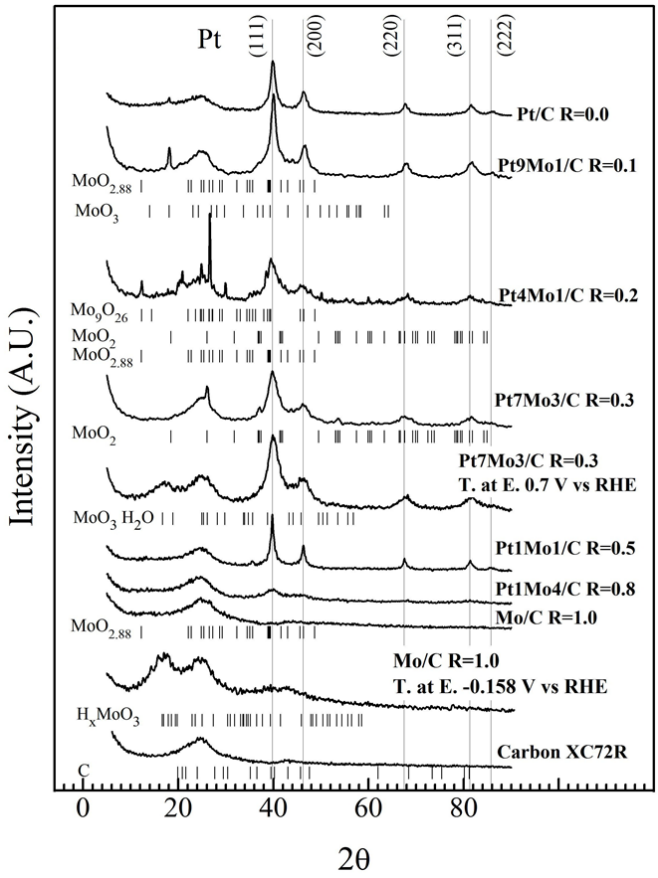

Figure 2. XRD of fresh PtMo/C series and electrochemically treated Pt7Mo3/C and Mo/C. The treatment was performed for 1 h at 0.7 V vs. NHE in a three-electrode cell with 0.5 M H_2SO_4 supporting electrolyte.

The intensity of these lines increases with the Pt content in the PtMo/C formulations without any evident displacement related to the incorporation of Mo into the Pt lattice. Different Mo oxides were detected in fresh PtMo/C materials. MoO_2 was observed (card 32-0671) in the Pt4Mo1/C, Pt7Mo3/C and Pt1Mo1/C electrocatalysts. Pt4Mo1/C also presented diffraction lines corresponding to Mo_9O_{26} (card 01-1194) and $MoO_{2.88}$. In the Pt9Mo1/C material it was also possible to detect $MoO_3 \bullet H_2O$. After electrochemical treatment for 1 h at 0.7 V vs. NHE, Pt7Mo3/C conserved the metallic Pt lines without any modification, whereas those corresponding to MoO_3 were replaced by the molybdenum bronze signals. Table 2 presents the lattice parameters and platinum crystallite size calculated by Bragg and Debye-Scherrer equations. The crystallite size ranges from 4.7 to 9.3 nm for PtMo/C materials, whereas for Pt/C it was 5.4 nm. No important changes were detected in the lattice parameter with the incorporation of molybdenum.

Table 2. Physical characterizations of PtMo/C series.

Electrocatalyst	XRD Pt Lattice parameter a (Å)	Crystallite size by XRD (nm)	Particle size by HRTEM (nm)	Pt $4f_{7/2}$ Binding energy (eV)
Pt/C R=0.0	3.9103	5.4	3	72.65
Pt9Mo1/C R=0.1	3.8933	4.7	N.D.	72.36
Pt4Mo1/C R=0.2	3.9504	2.7	3	72.54
Pt7Mo3/C R=0.3	3.9216	2.7	2	72.52
Pt1Mo1/C R=0.5	3.9216	9.3	3	72.32
Pt1Mo4/C R=0.8	3.9216	2.1	3	72.55
Mo/C R=1.0	N.D.	N.D.	2	N.D.

TEM images of the reference materials, Pt/C and Mo/C, as well as of the Pt7Mo3/C electrocatalyst are shown in Figure 3. These materials exhibit a homogeneous deposition of the metallic phases on the carbon support surface. Mo/C presents a main particle size of 2 nm (Figure 3a) and, in some particles it was possible to observe interplanar distances of 3.2, 3.3, 3.5, 3.6 and 3.8 Å, which are slightly smaller than those reported for the Mo-Mo bond (3.9 Å at the 220 plane) in the orthorhombic crystalline structure of MoO_3 [40, 44, 45]. This variation could be explained by the presence of different molybdenum oxides, just as was observed by XRD. For the Pt/C material, the main particle size registered was 3 nm, although some agglomeration can be found (Figure 3b). The corresponding planes of the fcc lattice are observed with interplanar distances of 2.8 Å (plane 220), similar to that of 2.77 Å reported in other studies [46, 47]. Pt7Mo3/C (Figure 3c) and the rest of the PtMo/C series showed the same characteristics as the reference materials: active phases homogeneously dispersed and small particle sizes, which are in accordance with those calculated by XRD (Table 2).

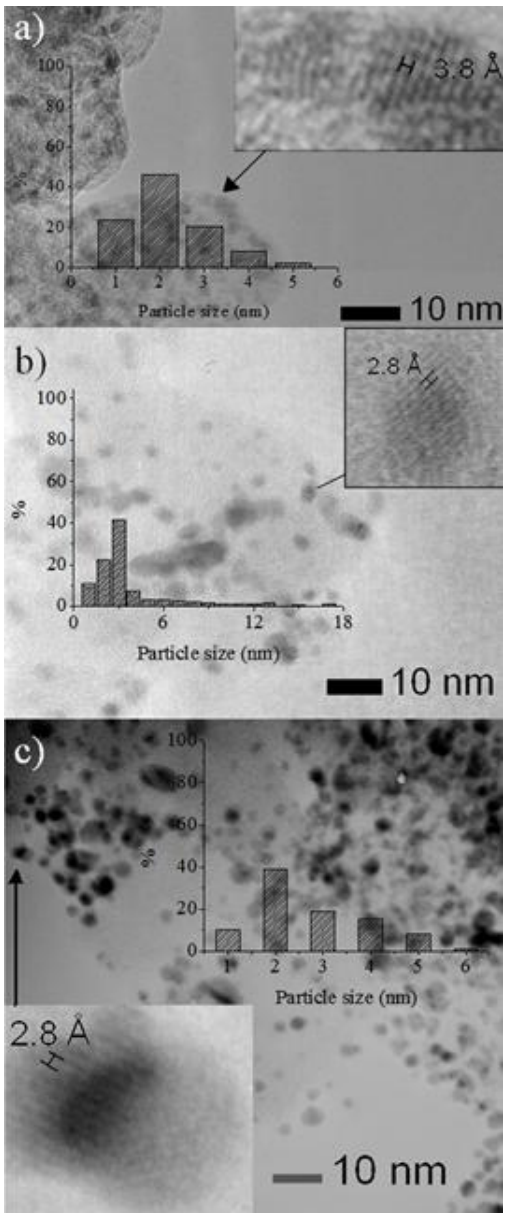

Figure 3. HRTEM of a) Mo/C, b) Pt/C and c) Pt7Mo3/C electrocatalysts.

In order to corroborate the molybdenum distribution along the support surface, Z-contrast images were recorded for Pt1Mo1/C and Pt1Mo4/C electrocatalysts (Figure 4). Two types of particles are distinguished: bright particles with sizes between 8 and 10 nm; and small, opaque particles of around 3 nm. The brightest particles are those with the highest atomic mass, in this case Pt. XEDS elementary analyses of the two types of particles are presented in Figure 5. The presence of Pt and Mo was confirmed in the small-particle region. Molybdenum is likely decorating and stabilizing the Pt particle size and avoiding the sinterization process. Only Pt was detected in large particles. Perhaps no Mo surrounded the Pt particles, which grew and reached sizes from 8 to 13 nm during the thermolysis process. Similar behavior was observed for the Pt1Mo4/C electrocatalysts.

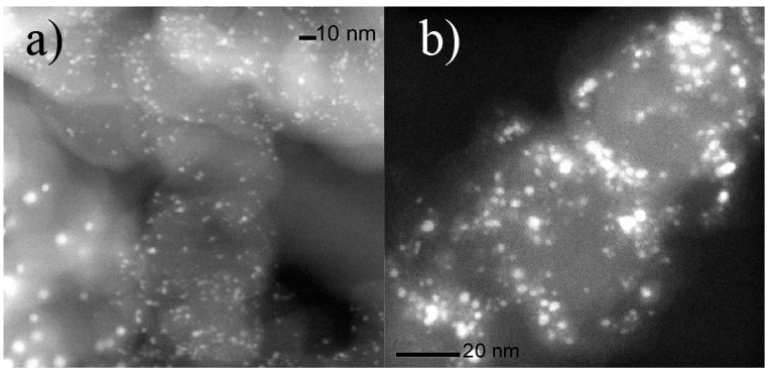

Figure 4. Z-contrast image of a) Pt1Mo1/C and b) Pt1Mo4/C electrocatalysts.

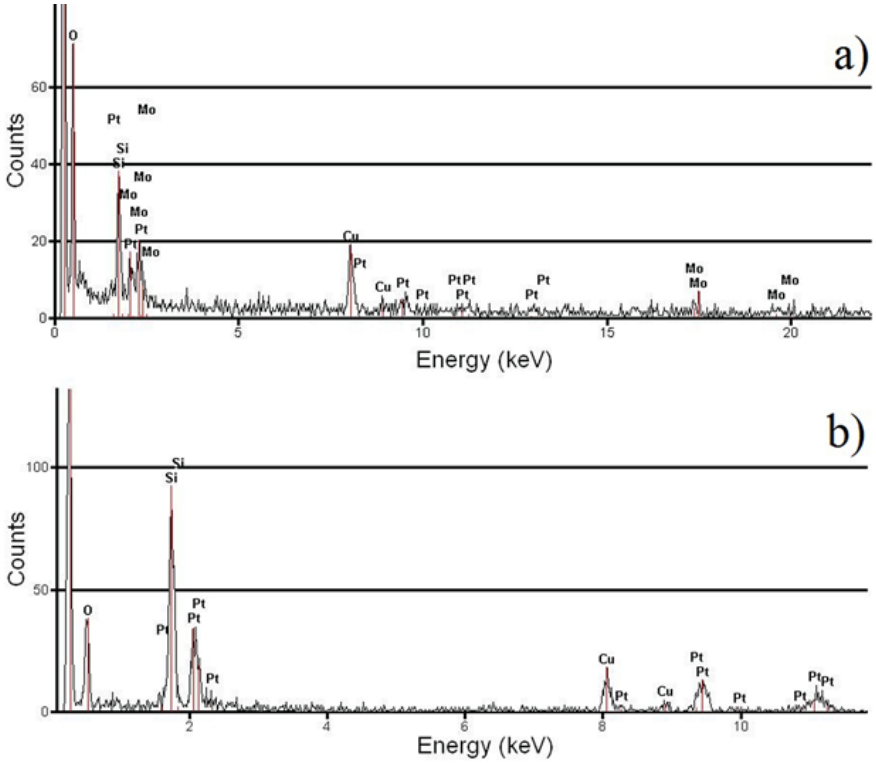

Figure 5. XEDS microanalysis of Pt1Mo1/C: a) small particles (~ 2 nm), b) large particles (~ 10 nm).

XPS spectra of the entire PtMo/C series (Figure 6a) showed the presence of the Pt $4f_{7/2}$ peak at 72.65 eV corresponding to the Pt $4f_{7/2}$ - Pt $4f_{5/2}$ doublet, the Mo $3d_{5/2}$ peak at 229.06 eV related to the Mo $3d_{5/2}$ - Mo $3d_{3/2}$ doublet, carbon C 1s at 285 eV and Oxygen O 1s at 531 eV. The signal intensities of Pt and Mo increase as the content of each one of these elements is increased in the formulation. Comparatively, the intensity of the carbon support signal (C 1s) is high, masking Pt and Mo. Satellite peaks of carbon and oxygen can also be seen because the source used is not monochromatic. Argon is also visible, possibly due to its adsorption during the erosion process while it was being used to clean the surface of the sample.

High resolution spectra for the Pt 4f region, ($Pt4f_{7/2}$ and $Pt4f_{5/2}$ doublet) [48], revealed the presence of metallic Pt in the whole PtMo/C series (Figure 6b). The position of the $Pt4f_{7/2}$ peak does

not present a clear trend with respect to the Mo content in the formulation. However, all PtMo/C samples presented slight displacements towards smaller binding energies compared with Pt/C (Table 2). The maximum peak position depends, to a certain degree, on the chemical environment of the atom responsible for the peak. The variation in the number of valence electrons and the bond type influence the binding energy of the inner electrons. The presence of molybdenum decorating Pt particles is expected to cause a displacement towards smaller binding energies, due to an increase in the electronic density, thereby decreasing the attraction of the nuclei to the inner-layer electrons. In the Mo3d doublet region, the best signal resolution was obtained in the samples with high Mo content. The high resolution XPS spectra for the $Mo3d_{5/2}$ - $Mo3d_{3/2}$ doublet (Figure 6c) showed wide peaks, indicating the presence of molybdenum species with different oxidation states. De-convolution analysis makes it possible to propose the presence of Mo(IV) $Mo3d_{5/2}$: 229.06 eV, Mo(V) Mo $3d_{5/2}$: 230.77 eV and Mo(VI) Mo $3d_{5/2}$: 232.80 eV. In the O 1s region, oxides of Mo (IV), Mo (V) and Mo (VI) appear between 531.02 to 531.82 eV. Additionally, a well-defined peak assigned to C = 0 species is presented at 533.54 eV (Figures 6d) [49].

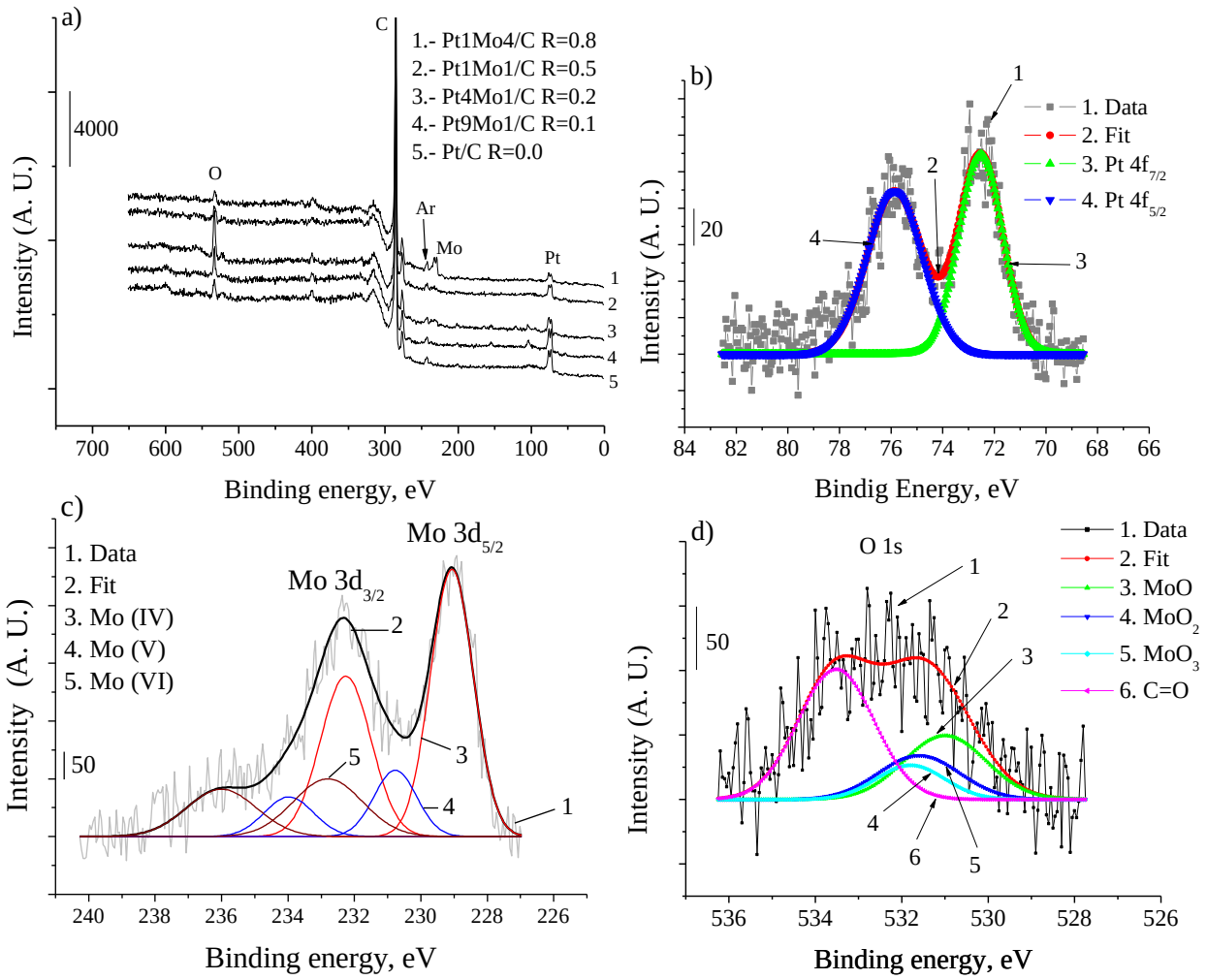

Figure 6. a) Wide-range XPS spectrum of PtMo/C series. XPS analysis for Pt1Mo4/C electrocatalyst at: b) Pt4f, c) Mo_{3d} and d) O 1s regions.

3.2 Electrochemical measurements

Figure 7 presents the forward scans of the CO stripping tests for both series: PtMo/C and mechanical mixtures. The entire cycles are inserted in Figure 7a. For Pt/C, a first shoulder appears at 0.69 V, which corresponds to the oxidation of weakly bridged CO adsorbed onto the Pt surface. The main peak potential for the strongly adsorbed CO species is located at 0.79 V. The molybdenum-containing series only presents the oxidation peak of strongly adsorbed CO [50] and the onset potential is shifted toward smaller potentials as the molybdenum content decreases. In the cases of Pt4Mo1/C and Pt7Mo3/C, CO oxidation respectively starts at potentials 100 mV and 130 mV lower than on platinum alone. Meanwhile, for the M2 mechanical mixture, it is found at a potential 120 mV lower. These results indicate that Mo does not have the capability to adsorb or oxidize CO, but its presence in small proportions in the electrocatalyst formulation diminishes the required energy for CO oxidation [51-53]. Similarities between PtMo/C and the mechanical mixtures series show that Mo and Pt sites do not necessarily have to be in an adjacent arrangement, as intended in the bifunctional mechanism for the PtRu system [6, 7, 23, 46, 54]. The interaction between both Mo and Pt sites could be explained by the diffusion of oxygen-containing species over the support surface, from the molybdenum bronze to the CO-poisoned platinum site. The possibility that protons exchange between Pt-H species and molybdenum bronzes has also been proposed [30-32, 34, 35]. This would mean that there would be a higher number of available Pt sites to adsorb and oxidize CO. Table 1 presents the catalytic active area, calculated from the electrical charge of the CO oxidation peak. The PtMo/C series showed higher catalytic areas than Pt/C. The opposite is seen in the mechanical mixtures.

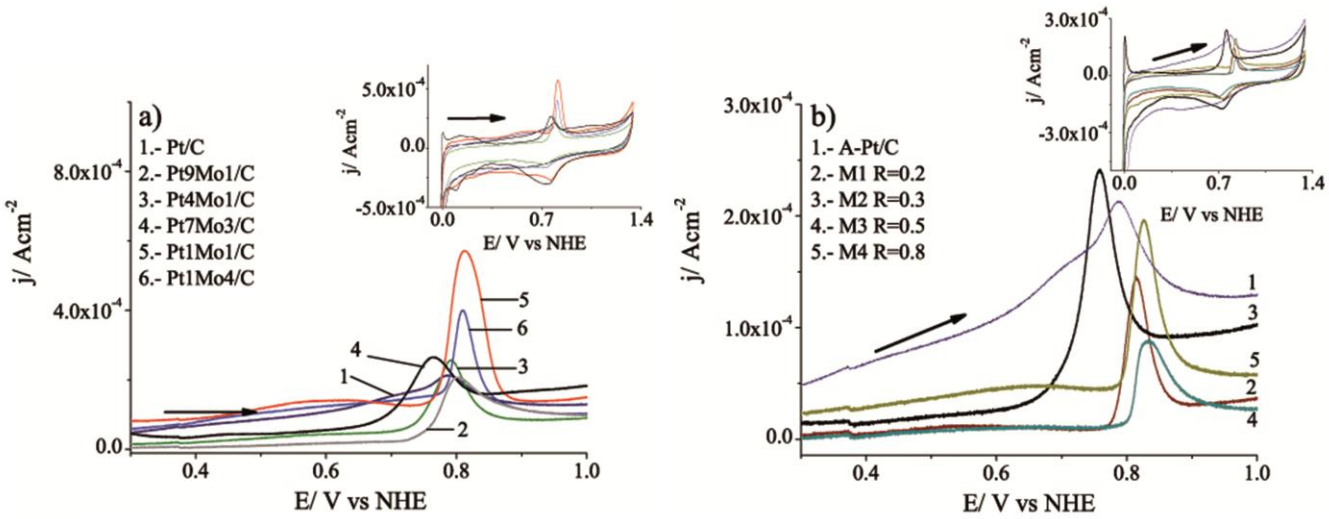

Figure 7. CO stripping voltammetry of (a) PtMo/C and (b) mechanical mixtures series.

The methanol electro-oxidation reaction was studied in quasi-steady state in order to observe faradaic processes occurring at the working electrode. In a window set between 0 and 1.2 V vs. NHE, potential steps were applied every 100 mV during 3 minutes, and current was registered after it was stabilized. Figure 8 presents the obtained current-sampled voltammetry curves for the PtMo/C series.

Methanol oxidation takes place between 0.3 and 0.9 V vs. NHE. From 0.9 V onwards, the oxidation peak of intermediate species is observed.

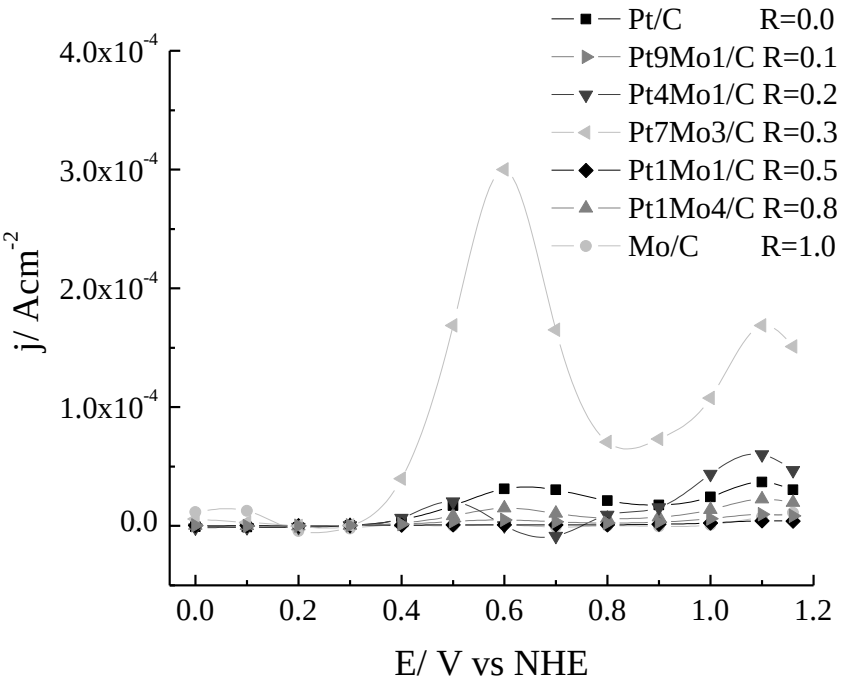

Figure 8. Steady-state voltammetry of PtMo/C series.

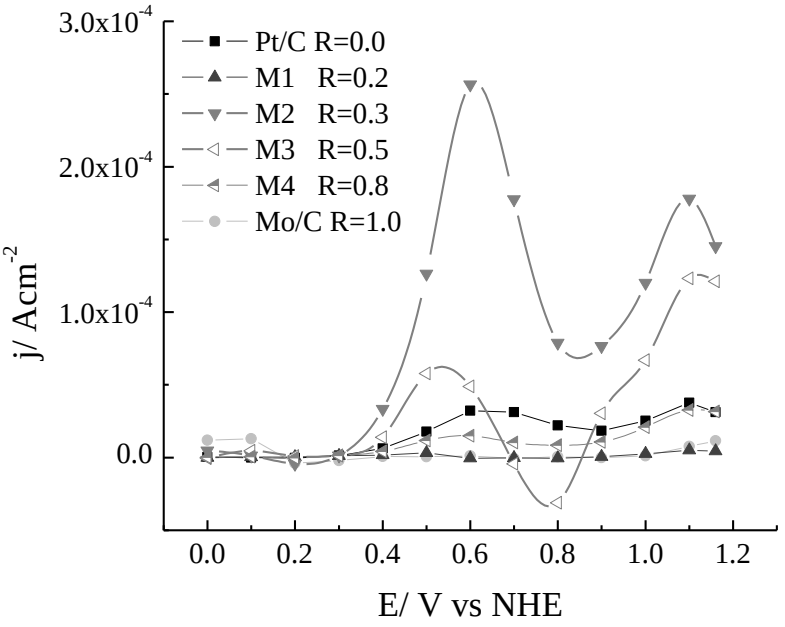

Figure 9. Steady-state voltammetry of mechanical mixtures series.

At higher potentials, oxygen evolution occurs. The Pt7Mo3/C electrocatalyst presented the lowest onset potential and the highest current for methanol electro-oxidation. Pt4Mo1/C and Pt9Mo1/C

also showed lower onset and peak potentials than Pt/C, whereas samples with higher Mo content registered an important decrease in the current response. This could be related to the fact that a lower number of platinum sites are available in these catalysts, perhaps because Mo phases could be deposited over them. Similar results were registered for the mechanical mixtures series (Figure 9). The M2 R = 0.3 and M = 0.5 samples presented lower onset potentials and higher currents than Pt/C. All series presented lower main methanol oxidation peak potentials than Pt/C (at a potential 100 mV lower in M2 and M3 mixtures). Current-sampled voltammetry results clearly confirm that the best promoting effect is obtained at low Mo contents and that it is not necessary to have Mo particles adjacent to Pt sites in order to increase the activity towards methanol electro-oxidation, as proposed in the bifunctional mechanism model. The Mo promoting effect could be related to a surface diffusion mechanism in which oxygen-containing species migrate from Mo bronzes ($HxMoO_3$) to Pt sites throughout the carbon surface. Adsorbed intermediate species would be oxidized leaving a higher number of available Pt sites for methanol electro-oxidation.

4. CONCLUSIONS

PtMo/C and mechanical mixtures of Pt/C + Mo/C were prepared by the metal carbonyl thermolysis synthesis method. The active phase was homogeneously dispersed onto the support surface with average particle sizes between 2 and 3 nm. XPS and XRD results for fresh materials indicate the presence of metallic platinum and molybdenum oxides with different oxidation states: Mo(IV), Mo(V) and Mo(VI). However, XRD analyses, performed after different electrochemical treatments, indicate that in reaction conditions the active phase was composed of metallic platinum and molybdenum bronzes ($HxMoO_3$). These bronzes are present in the entire potential range in which the methanol oxidation reaction was studied. Molybdenum bronzes (H_xMoO_3) do not participate directly as catalysts in methanol or CO oxidation. However, a molybdenum-modified platinum catalyst presented higher activity for methanol oxidation compared with Pt/C, indicating the activity promoting role of H_xMoO_3. The most significant promoting effect was found with Mo/(Mo+Pt) atomic ratios of 0.3 and 0.2. The increase in methanol oxidation activity was also observed with Pt/C + Mo/C mechanical mixtures, materials where the Pt and Mo sites are surely separated. It confirms the existence of a remote promoting effect, related to the presence of molybdenum bronzes in the catalyst formulation. Thus, it is not necessary to have adjacent Pt and Mo sites in order to obtain an improvement in activity.

ACKNOWLEDGEMENTS
The authors thank Ivan Puente Lee, Manuel Aguilar Franco and Lazaro Huerta for their technical assistance with the microscopy imaging, XRD analysis and XPS experiments respectively. The authors acknowledge the financial support for this work from CONACYT 181106 and PAPIIT 103410.

References

1. C. Lamy, E.M. Belgsir, J.M. Léger, *J Appl Electrochem*, 31 (2001) 799.
2. Y. Zhu, H. Uchida, T. Yajima, M. Watanabe, *Langmuir*, 17 (2000) 146.

3. Y.X. Chen, A. Miki, S. Ye, H. Sakai, M. Osawa, *J Am Chem Soc*, 125 (2003) 3680.
4. M. Götz, H. Wendt, *Electrochim Acta*, 43 (1998) 3637.
5. T. Frelink, W. Visscher, J.A.R. Van Veen, *Surf Sci*, 335 (1995) 353.
6. M. Watanabe, S. Motoo, *J Electroana Chem*, 60 (1975) 267.
7. M. Watanabe, S. Motoo, *J Electroana Chem*, 60 (1975) 275
8. G. Samjeské, H. Wang, T. Löffler, H. Baltruschat, *Electrochim Acta*, 47 (2002) 3681.
9. B.N. Grgur, N.M. Markovic, P.N. Ross, *J Electrochem Soc*, 146 (1999) 1613.
10. A. Oliveira Neto, E.G. Franco, E. Aricó, M. Linardi, E.R. Gonzalez, *J Eur Ceram Soc*, 23 (2003) 2987.
11. S. Mukerjee, R.C. Urian, *Electrochim Acta*, 47 (2002) 3219.
12. E. Teliz, V. Díaz, I. Pérez, M. Corengia, C.F. Zinola, *Int J Hydrogen Energ*, 37 (2012) 14761.
13. C. Huei-Yu,.Y. Tsung-Kuang, T. Chuen-Horng, *Int J Electrochem Sci*, 9 (2014) 5763.
14. S. Bong, B. Jang, S. Woo, Y. Piao, *Int J Electrochem Sci*, 8 (2013) 7510.
15. C. Lu, C. Rice, R.I. Masel, P.K. Babu, P. Waszczuk, H.S. Kim, E. Oldfield, A. Wieckowski, *J Phys Chem B*, 106 (2002) 9581.
16. T.E. Shubina, M.T.M. Koper, *Electrochim Acta*, 47 (2002) 3621.
17. M. Arenz, V. Stamenkovic, B.B. Blizanac, K.J. Mayrhofer, N.M. Markovic, P.N. Ross, *J Catal*, 232 (2005) 402.
18. J.L. Gómez de la Fuente, M.V. Martínez-Huerta, S. Rojas, P. Hernández-Fernández, P. Terreros, J.L.G. Fierro, M.A. Peña, *Appl Catal B-Environ*, 88 (2009) 505.
19. L.C. Ordóñez, P. Roquero, P.J. Sebastian, J. Ramírez, *Catal Today*, 107–108 (2005) 46.
20. P. Roquero, L. C. Ordóñez, O. Herrera, O. Ugalde, J. Ramírez, *Int J Chem React Eng*, 5 (2007) 1542.
21. L.C. Ordóñez, P. Roquero, P.J. Sebastian, J. Ramírez, *Int J Hydrogen Energ*, 32 (2007) 3147.
22. H.D. Herrera-Méndez, P. Roquero, M. A Smit, L. C. Ordóñez, *Int J Electrochem Sci*, 6 (2011) 4454.
23. J.A. Shropshire, *J Electrochem Soc*, 112 (1965) 465.
24. H. Zhang, Y. Wang, E.R. Fachini, C.R. Cabrera, *Electrochem Solid State Lett*, 2 (1999) 437.
25. D.M. Dos Anjos, K.B. Kokoh, J.M. Léger, A.R.D. Andrade, P. Olivi, G. Tremiliosi-Filho, *J Appl Electrochem*, 36 (2006) 1391.
26. A.C.R. Aguiar, P. Olivi, *J Power Sources*, 195 (2010) 3485.
27. E.I. Santiago, G.A. Camara, E.A. Ticianelli, *Electrochim Acta*, 48 (2003) 3527.
28. R. Prins, *Chem Rev*, 112 (2012) 2714.
29. W.C. Conner, J.L. Falconer, *Chem Rev*, 95 (1995) 759.
30. V.V. Rozanov, O.V. Krylov, *Russ Chem Rev*, 66 (1997) 107.
31. R. Green, P. Morrall, M. Bowker, *Catal Lett*, 98 (2004) 129.
32. X. Xiang, W. Li, Z. Zhou, Z. Fu, J. Lei, Y. Lin, *J Solid State Electr*, 14 (2010) 903.
33. X. Wang, W. Wu, X. Xiang, W. Li, *J Power Sources*, 259 (2014) 255.
34. Z.H. Zhou, W.S. Li, Z. Fu, X.D. Xiang, *Int J Hydrogen Energ*, 35 (2010) 936.
35. X.D. Xiang, Q.M. Huang, Z. Fu, Y.L. Lin, W. Wu, S.J. Hu, W.S. Li, *Int J Hydrogen Energ*, 37 (2012) 4710.
36. W. Li, J. Lu, J. Du, D. Lu, H. Chen, H. Li, Y. Wu, *Electrochem Commun*, 7 (2005) 406.
37. P.K. Shen, A.C.C. Tseung, *J Electrochem Soc*, 141 (1994) 3082.
38. Y. Iizuka, *Stud Surf Sci Catal*, 77 (1993) 317.
39. K. Eda, N. Sotani, M. Kunitomo, M. Kaburagi, *J Solid State Chem*, 141 (1998) 255.
40. R.C.T. Slade, T.K. Halstead, P.G. Dickens, R.H. Jarman, *Solid State Commun*, 45 (1983) 459.
41. P.G. Dickens, R.H. Jarman, R.C.T. Slade, C.J. Wright, *J Chem Phys*, 77 (1982) 575.
42. C. Ritter, W. Müller-Warmuth, R. Schöllhorn, *J Chem Phys*, 83 (1985) 6130.
43. S.P. Mehandru, A.B. Anderson, *J Am Chem Soc*, 110 (1988) 2061.
44. S.P. Mehandru, A.B. Anderson, *J Am Chem Soc*, 110 (1988) 2061.

45. S. Adams, *J Solid State Chem*, 149 (2000) 75.
46. S. Mukerjee, J. McBreen, *J Electroanal Chem*, 448 (1998) 163.
47. R.C. Urian, A.F. Gullá, S. Mukerjee, *J Electroanal Chem*, 554–555 (2003) 307.
48. S.C. Hall, V. Subramanian, G. Teeter, B. Rambabu, *Solid State Ionics*, 175 (2004) 809.
49. Nist XPS Database. http://srdata.nist.gov/xps/
50. D.C. Papageorgopoulos, M. Keijzer, F.A. de Bruijn, *Electrochim Acta*, 48 (2002) 197.
51. O. Guillén-Villafuerte, R. Guil-López, E. Nieto, G. García, J.L. Rodríguez, E. Pastor, J.L.G. Fierro, *Int J Hydrogen Energ*, 37 (2012) 7171.
52. V. Martínez-Huerta, J.L. Rodríguez, N. Tsiouvaras, M.A. Peña, J.L.G. Fierro, E. Pastor, *Chem Mater*, 20 (2008) 4249.
53. V. Kaydashev, E. Janssens, P. Lievens, *Int J Mass Spectrom*, 379 (2015) 133.
54. M.V. Martínez-Huerta, J.L. Rodríguez, N. Tsiouvaras, M.A. Peña, J.L.G. Fierro, E. Pastor, *Chem Mater*, 20 (2008) 4249.